Desalination 286 (2012) 400–411

Contents lists available at SciVerse ScienceDirect

Desalination

journal homepage: www.elsevier.com/locate/desal

Experimental and simulation study of a solar thermal driven membrane distillation desalination process

Hsuan Chang *, Shao-Gang Lyu, Chih-Ming Tsai, Yih-Hang Chen, Tung-Wen Cheng, Ying-Hsiu Chou

Energy and Opto-Electronic Materials Research Center, Department of Chemical and Materials Engineering, Tamkang University, New Taipei City, Taiwan

ARTICLE INFO

Article history:
Received 24 September 2011
Received in revised form 28 November 2011
Accepted 29 November 2011
Available online 4 January 2012

Keywords:
Membrane distillation
Desalination
Modeling
Solar energy
Optimization
Process control

ABSTRACT

Being capable of directly utilizing solar thermal energy, the solar membrane distillation desalination system (SMDDS) has evolved as a promising green technology for alleviating the water resource problem. This paper reports the experimental and simulation study of a SMDDS which utilizes the air gap type membrane distillation. A laboratory system with automatic control function was established. A control scheme for fully automatic operation was designed using the PI (proportional–integral) control algorithm, which is robust and commonly employed by industries. The control structure adopted PI temperature control for the solar thermal and the membrane distillation subsystems. A dynamic mathematical model including the control algorithm for the overall system was developed, built on Aspen Custom Modeler® platform, and verified by the experimental results. The optimization analysis using the model reveals the operation strategy for maximum water production. Because of the unpredictable solar irradiation, the corresponding optimal dynamic operation cannot be predetermined and implemented during system operation. However, the proposed PI control scheme could provide a fairly good level of performance, for example up to about 80% of the maximum water production for sunny day operation.

1. Introduction

Membrane distillation (MD) is a thermally driven process, in which only vapor molecules are transported through hydrophobic micro-porous membranes. Desalination is a major application of MD and the configurations commonly employed are direct contact (DCMD) and air gap (AGMD). Utilization of renewable energy for desalination is a green solution for the problem of water resource. MD has the advantages of simplicity and can operate with low grade thermal energy. The solar driven MD desalination system, where energy is supplied entirely by flat-plate solar thermal collectors and PV panels, has been investigated in many important aspects, including the feasibility, design of membrane distillation module, energy consumption, and economic analysis, by several research institutions [1–6]. The system modeling, control and optimization are less explored.

On the modeling and control of the solar powered desalination processes, Ben Bacha et al. [7] and Roca et al. [8] presented studies for a solar multiple condensation evaporation cycle system and a hybrid solar-fossil fuel powered multi-effect distillation system, respectively. Both groups developed reduced process models for incorporating with their proposed control algorithms based on linear control technique and feedback linearization technique, respectively. Bacha et al. [1,2] and Guillén-Burrieza et al. [5] reported plant operation performance of solar powered MD desalination.

In this paper, we present a laboratory-scale solar thermal driven membrane distillation experimental system with control design as well as a dynamic model for the system and the verification using the experimental results. Using the model, the optimal dynamic operation profiles reveal the optimal operation strategy and allow the evaluation of the performance of automatic control operation.

2. Experimental setup and operation

The experimental setup of a SMDDS system is illustrated in Fig. 1. Fig. 1(a) depicts the flow sheet and Fig. 1(b) shows the picture of the equipments. The major equipments include a hot thermostat, a thermal storage tank, a counter-flow shell and tube heat exchanger, an AGMD, peristaltic pumps (Baoding Longer, BT600-2J) and a cold thermostat. The solar absorber is simulated using the hot thermostat which provided pre-set thermal energy according to the specified solar irradiation profiles. For reducing the experimental time, the one-day (24 h) solar irradiation profiles are contracted into 6 h, the profiles for sunny day and cloudy day are shown in Fig. 2. With the stair-shape profiles, it is easy to operate the hot thermostat to provide the corresponding heating loads. In this study, deionized water, instead of sea water, was used. The temperature of cold water feed is fixed using a cold thermostat. The thermal storage circulation fluid, which absorbs thermal energy from the solar absorber, is split into two parts. One part is fed into a thermal storage tank prior to

* Corresponding author. Tel.: +886 2 26232094; fax: +886 2 26209887.
E-mail address: nhchang@mail.tku.edu.tw (H. Chang).

0011-9164/$ – see front matter © 2011 Elsevier B.V. All rights reserved.
doi:10.1016/j.desal.2011.11.057

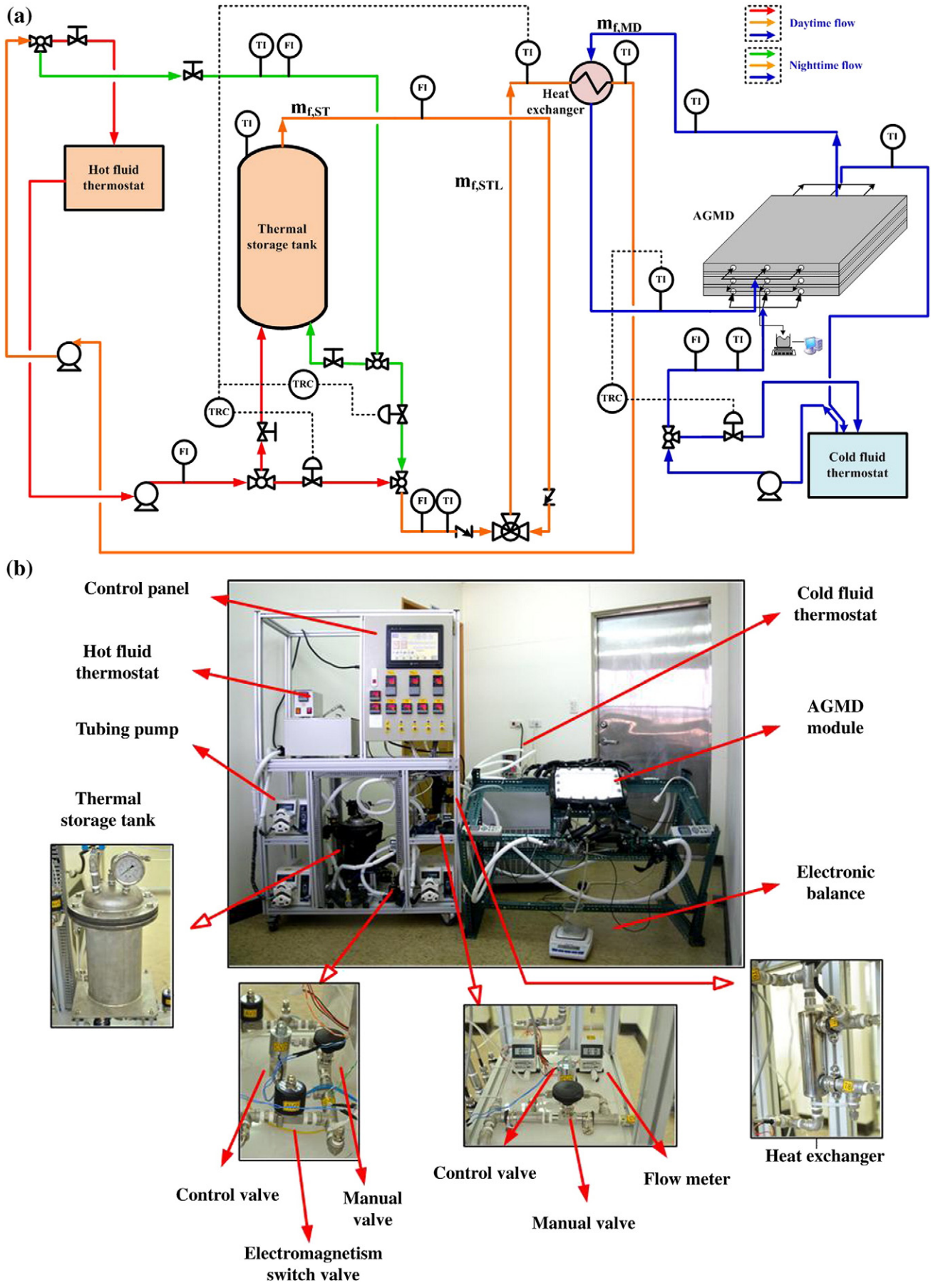

Fig. 1. Experimental setup.

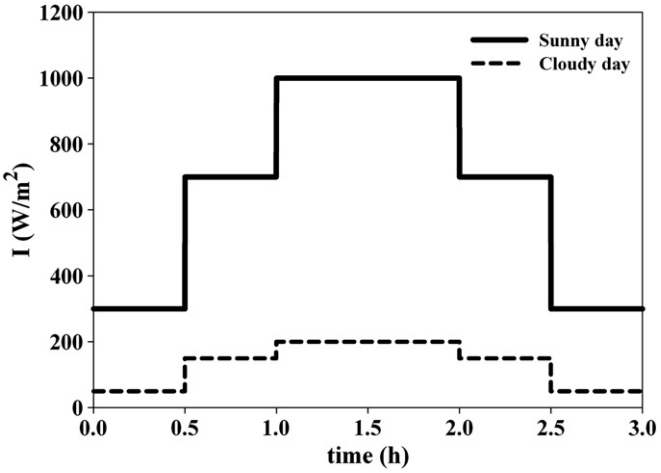

Fig. 2. Solar irradiation profiles.

entering the heat exchanger and the other part is directly fed into the heat exchanger. The splitting ratio is determined with a fixed (manual operation) or controller adjusted (automatic operation) manner. The flat plate AGMD module is designed with energy recovery function. The cold feed water is first heated in the module by energy exchange with the hot fluid, then further heated in the heat exchanger and returned to the hot side of the module as the hot fluid feed. The module has an inclination angle of 27° to the horizon for easy collection of the condensed permeate and both hot and cold fluids flow upward to ensure complete filling of the flow channels. The condensed permeate, that is the water transported through the membrane, is collected and measured for its temperature and cumulative mass with a thermocouple sensor and an electronic balance (Precisa, BJ 610C). Major equipments as well as the connecting tubing are insulated to reduce heat loss to the environment. The details of equipment specifications are summarized in Table 1.

The control system, also shown in Fig. 1(a), consists of three temperature control loops. Two of them are used to control the hot fluid temperature entering the heat exchanger, one for daytime operation and the other one for nighttime operation. The inlet flow rate to the thermal storage tank is the manipulated variable. The third control loop adjusts the membrane distillation flow rate to control the hot fluid temperature entering the AGMD module. The control loop employs the microprocessor PID temperature controller (Hunjoen Electronic Co., Ltd., H-D96H) and the PSV proportional solenoid valve (Aalborg Instruments & Controls, Inc.). As shown in Fig. 1(a), flow and temperature measurements are allocated for major streams. All measured dynamic data, including temperature, flow rate and cumulative water production, are recorded in a micro computer.

The experiments are performed under manual or automatic operations for different specified circulation flow rate of solar thermal loop ($m_{f,STL}$), ranging 4.6–5.2 kg/h. Under manual operation, the ratio of flow entering thermal storage tank ($r_{f,ST} = m_{f,ST}/m_{f,STL}$) is specified, ranging 0.5–0.9, and the hot fluid flow rate of AGMD module ($m_{f,MD}$) is specified too, ranging 2.2–2.8 kg/h. For automatic control, $r_{f,ST}$ and $m_{f,MD}$ are adjusted by temperature controllers. Moreover, experiments are carried out under both sunny day and cloudy day solar irradiation conditions.

Before starting data recording for each experiment case, fluids are circulated in both loops, namely the solar thermal loop and the membrane distillation loop, to obtain the steady starting temperatures of 50 °C and 20 °C, respectively, with the operations of hot and cold thermostats. The experiment is then started by manually adjusting the hot thermostat to meet the specified solar irradiation profile. If the experiment is for automatic operation, each controller should be pre-set for the set point temperature and tuning parameters. Each experiment case are repeated for three times and compared for the measured data.

3. Simulation

As other thermal and chemical processes, the membrane distillation modules and desalination processes can be simulated by developing models on commercial process simulation software for easy study of unit and flow sheet design alternatives. Chang et al. [9–11] have reported model development as well as process analysis for DCMD, AGMD and solar driven desalination process on Aspen Plus® and Aspen Custom Modeler® [12] platforms.

Based on the model reported in our previous paper [10], equipment models of solar thermal energy supply unit and the AGMD unit are changed to meet the experimental set up. The solar thermal absorber is replaced by a thermostat which supplies hot fluid with a specified profile. The spiral wound AGMD unit is replaced by a flat plate AGMD module. The correlations of heat transfer coefficient employed are hence different. The models for equipments of SMDDS are described individually in this section. The dynamic model is built on the Aspen Custom Modeler® [12] platform, which allows convenient implementation of the flow sheet study, optimization analysis as well as control system design. For all the equipments, the energy balance considers the variation of temperature in the fluid flow direction, which means the model is one-dimensional. Mass balance analysis is needed for the AGMD module only and the model is also one-dimensional.

3.1. Models

Because the solar absorber is simulated with a thermostat, which provides thermal energy to the fluid according to a given solar irradiation profile, the energy balance equation for the fluid can be written as

$$\frac{\partial T_{f,SA}}{\partial t} = -L_{SA}\frac{m_{f,SA}}{M_{f,SA}}\frac{\partial T_{f,SA}}{\partial x} + \frac{A_{SA}I(t)}{M_{f,SA}Cp_f^L}. \quad (1)$$

Table 1
Equipment specifications.

Solar absorber	
Mass, $M_{f,SA}$ (kg)	1.4
Width, W_{SA} (m)	0.095
Length, L_{SA} (m)	0.76
Thermal storage tank	
Total mass of water, $M_{f,ST}$ (kg)	3
Height of tank, H_{ST} (m)	0.28
Heat exchanger	
Area, A_{HX} (m^2)	0.005
Length, L_{HX} (m)	0.15
Overall heat transfer coefficient, U_{HX} (W/m^2 K)	280
Membrane distillation module	
Hot fluid channel height, H_{HL} (mm)	2
Cold fluid channel height, H_{CL} (mm)	2
Air gap thickness, H_{AG} (mm)	2
Membrane area, A_m (m^2)	0.05
Membrane width, W_{mem} (m)	0.25
Membrane length, L_{mem} (m)	0.2
Membrane total thickness, δ_{MEM} (μm)	130
Membrane porous layer thickness, δ_{mem} (μm)	30
Membrane material	PTFE (porous); PP (supporting)
Membrane pore diameter, d_p (μm)	0.1
Membrane porosity, ε	0.72
Membrane tortuosity, τ	1.39

The fluid inside the thermal storage tank is assumed to be in plug flow, hence the temperature variation of the fluid is one-dimensional. With inlet flow rate of $m_{f,ST}$, the energy balance is

$$\frac{\partial T_{f,ST}}{\partial t} = -H_{ST}\frac{m_{f,ST}}{M_{f,ST}}\frac{\partial T_{f,ST}}{\partial x}. \quad (2)$$

The heat exchanger is counter flow with hot fluid sent from the solar absorber or thermal storage tank and cold fluid sent from the membrane distillation module. Based on the plug flow assumption and specified overall heat transfer coefficient, the energy balances for both fluids are given as

$$\frac{dT_{f,HX,HL}}{dt} = L_{HX}\frac{m_{f,HX,HL}}{M_{f,HX,HL}}\frac{\partial T_{f,HX,HL}}{\partial x} - \frac{A_{HX}U_{HX}}{M_{f,HX,HL}Cp_f^L}\left(T_{f,HX,HL} - T_{f,HX,CL}\right) \quad (3)$$

$$\frac{dT_{f,HX,CL}}{dt} = -L_{HX}\frac{m_{f,HX,CL}}{M_{f,HX,CL}}\frac{\partial T_{f,HX,CL}}{\partial x} + \frac{A_{HX}U_{HX}}{M_{f,HX,CL}Cp_f^L}\left(T_{f,HX,HL} - T_{f,HX,CL}\right). \quad (4)$$

For the AGMD module, a model considering the heat and mass transfers in each layer and at the interface between layers, as illustrated in Fig. 3, is developed. Mass balance equations are written for the hot fluid and the condensing liquid as Eqs. (5) and (6) as well as for the interface between membrane and air gap as Eq. (7).

$$\frac{dm_{f,MD,HL}}{dx} = -N_{mem}Mw_wL_{MD} \quad (5)$$

$$\frac{dm_{f,MD,CONL}}{dx} = -N_{ag}Mw_wL_{MD} \quad (6)$$

$$N_{mem} = N_{ag} \quad (7)$$

As given in Eqs. (8) and (9), the mass fluxes are determined by the effective mass transfer coefficients and pressure difference driving forces in the membrane and air gap layers. The mass transfer coefficients are determined using Eqs. (10) and (11). For the membrane, Kundsen diffusion and molecular diffusion are considered [13]. For the air gap, only molecular diffusion is considered. The diffusion induced convection is accounted for in the mass flux calculation [14].

$$N_{mem} = \frac{k_{mem}}{RT_{mem}}\left(P_{w,m1}^{sat} - P_{w,m2}\right) \quad (8)$$

$$N_{ag} = \frac{k_{ag}P_{ag}^T}{RT_{ag}P_{a,lm}}\left(P_{w,m2} - P_{w,lf}^{sat}\right) \quad (9)$$

$$k_{mem} = \frac{\varepsilon}{\tau}\left[\frac{1}{1/D_K + y_{air,lm}/D_m}\right]\frac{1}{\delta_{mem}} \quad (10)$$

$$k_{ag} = \frac{D_m}{\delta_{ag}} \quad (11)$$

The energy balances for hot and cold fluid channels, as given in Eqs. (12) and (13), take into account the convective heat transfer across the boundaries and the sensible heat effect. The sensible heat effect results from the energy flow associated with the mass flux between two boundary interfaces of different temperatures.

$$\frac{\partial T_{f,MD,HL}}{\partial t} = -L_{mem}\left[\frac{m_{f,MD,HL}}{M_{f,MD,HL}}\frac{\partial T_{f,MD,HL}}{\partial x} + \frac{W_{mem}}{M_{f,MD,HL}Cp_f^L}\left(Q_{h,HL} + Q_{N,HL}\right)\right] \quad (12)$$

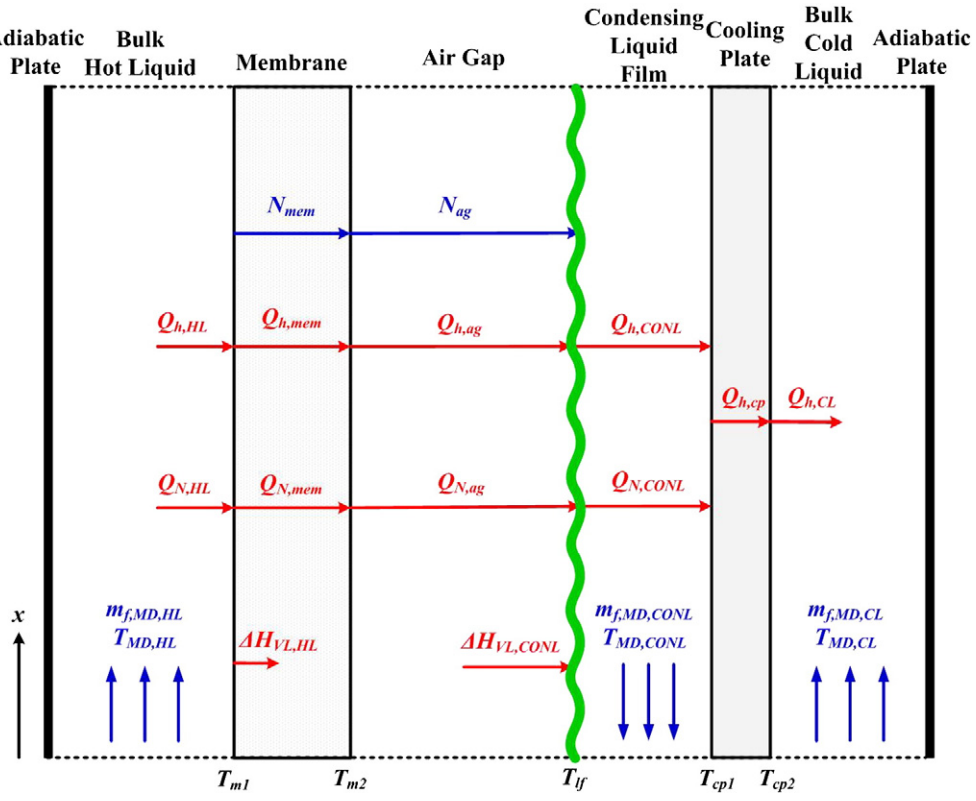

Fig. 3. Heat and mass transfers in AGMD.

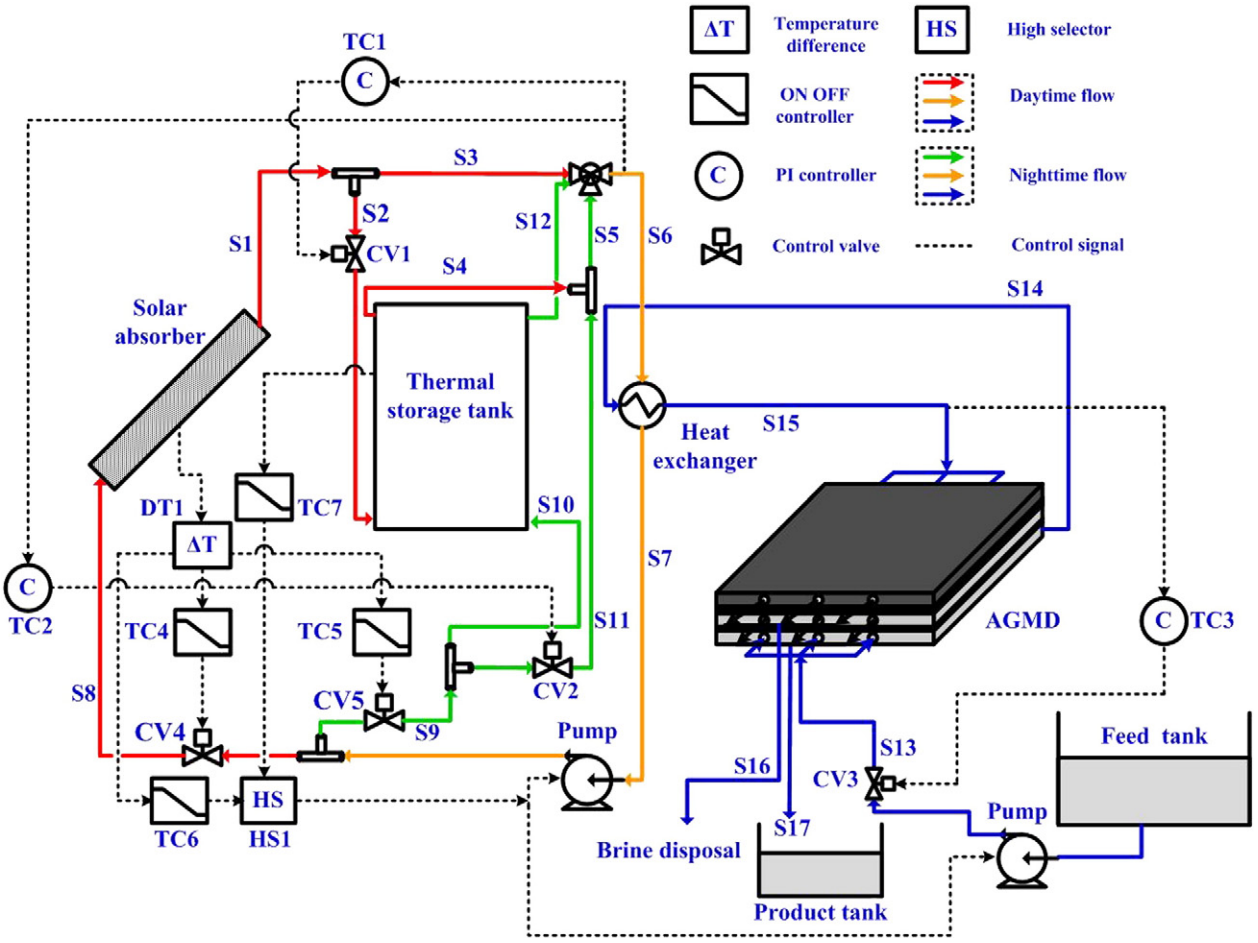

Fig. 4. Control system.

$$\frac{\partial T_{f,MD,CL}}{\partial t} = -L_{mem}\left[\frac{m_{f,MD,CL}}{M_{f,MD,CL}}\frac{\partial T_{f,MD,CL}}{\partial x} - \frac{W_{mem}}{M_{f,MD,CL}Cp_f^L}Q_{h,CL}\right] \quad (13)$$

For each interface, the heat effects on both sides should be balanced.

$$\begin{aligned} &Q_{h,HL} + Q_{N,HL} - \Delta H_{VL,HL} = Q_{h,mem} + Q_{N,mem} = Q_{h,ag} + Q_{N,ag} \\ &= Q_{h,CONL} + Q_{N,CONL} - \Delta H_{VL,CONL} = Q_{h,cp} - \Delta H_{VL,CONL} \\ &= Q_{h,CL} - \Delta H_{VL,CONL} \end{aligned} \quad (14)$$

The heat fluxes are determined by the heat transfer coefficients or heat of vaporization.

$$Q_{h,j} = h_j \Delta T_j \quad (15)$$

$$Q_{N,j} = N_j Cp_f \Delta T_j \quad (16)$$

$$\Delta H_{VL,j} = N_j \Delta H_{vap} \quad (17)$$

Considering the short flat plate module, the heat transfer coefficients for hot fluid and cold fluid channels are estimated using the correlation by Sieder and Tate for laminar flow through a circular channel [15] using equivalent hydraulic diameter of the flow channel. For the liquid film, the heat transfer coefficient is determined using the correlation of condensing film [15]. For the membrane, air gap and cooling plate, the heat transfer coefficients are determined using the thermal conductivity and thickness of the layer.

Table 2
Control devices and settings.

Devices	Device input or controlled variable	Set point	Device output or manipulated variable	Final control element
TC1 (PI controller)	T_{S6}	52 °C	$m_{f,S2}$	CV1
TC2 (PI controller)	T_{S6}	51 °C	$m_{f,S11}$	CV2
TC3 (PI controller)	T_{S15}	45 °C or 40 °C	$m_{f,S13}$	CV3
TC4 (ON/OFF controller)	ΔT_{SA}	0 °C	$m_{f,S8}$	CV4 (opened when $\Delta T_{SA} > 0$)
TC5 (ON/OFF controller)	ΔT_{SA}	0 °C	$m_{f,S9}$	CV5 (closed when $\Delta T_{SA} > 0$)
TC6 (ON/OFF controller)	ΔT_{SA}	0 °C	HS1	Pumps (opened when $\Delta T_{SA} > 0$)
TC7 (ON/OFF controller)	T_{ST}	50 °C	HS1	Pumps (opened when $T_{ST} > 50$ °C)
DT1 (Temperature difference)	ΔT_{SA}		TC4, TC5, TC6	
HS1 (high selector)	Output signals from TC6 and TC7			Pumps

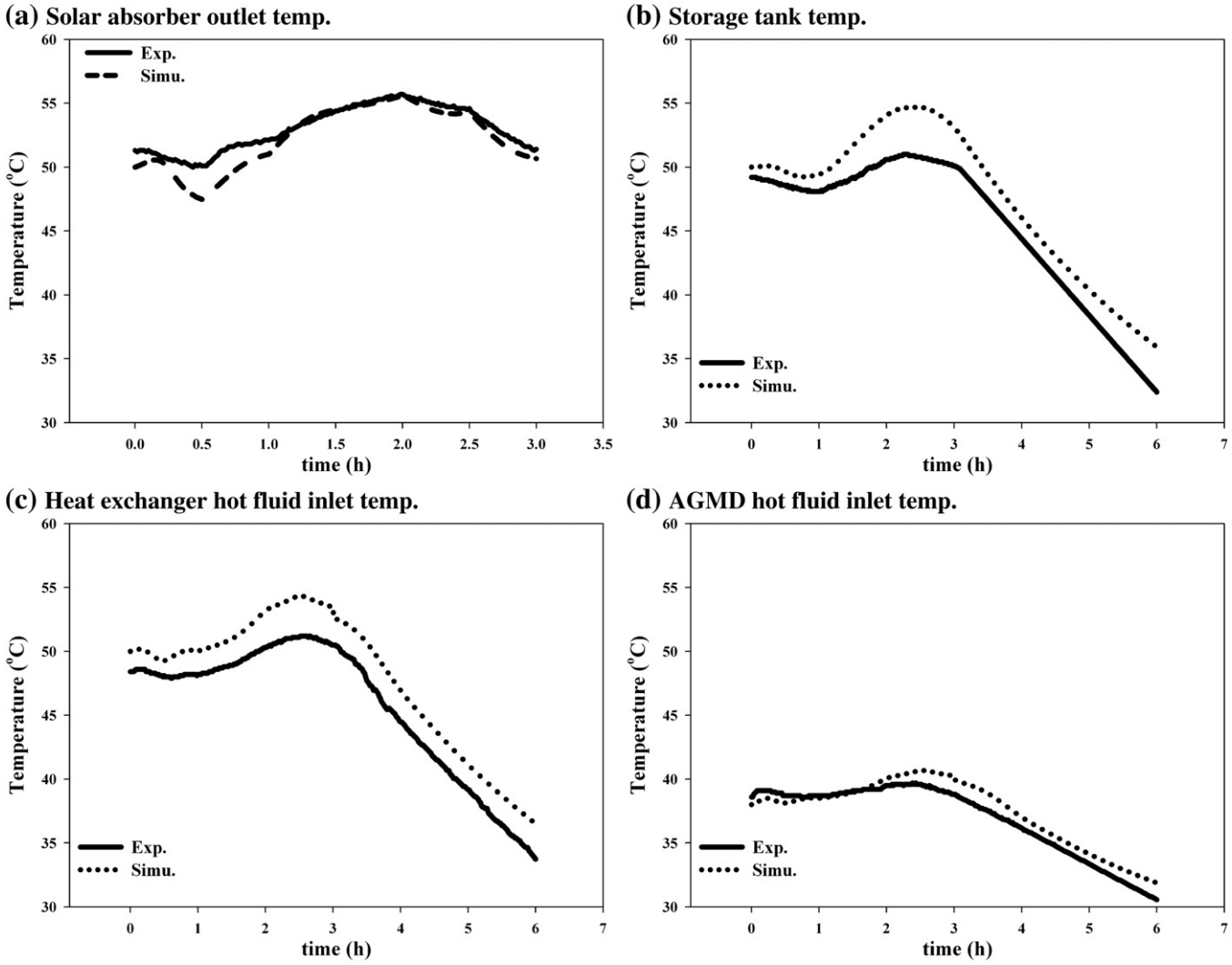

Fig. 5. Base case temperature profiles for sunny day.

3.2. Method of solution

The model is built on Aspen Custom Modeler® [12] platform and solved using the built-in solver. The partial differential equations are transformed into differential algebraic equations using method of lines first and then solved by Newton's method.

4. Control structure

For the control of water desalination industry using traditional energy sources, where steady state operation is attainable, two review papers concluded that classical PID (Proportional–Integral–Derivative) control system is the most recognized by the industry and in general has proven to be robust compared to the various modern control systems [16,17]. Base on predictive models, modern control algorithms can be employed to obtain optimal operations of systems. However, due to the unpredictable nature of the solar irradiation, the optimal operation and the corresponding target control states of the solar driven desalination process cannot be predicted. In this study, the PI control algorithm is adopted.

PID is the most commonly used feedback controller. A PID controller calculates an "error" value (E) as the difference between a measured process variable and a desired set point. The controller output (OP), which is the control action on the manipulated variable, is determined by the proportional (P), integral (I) and derivative (D) operations on the "error" as given in Eq. (18).

$$OP = K_c\left(E + \frac{1}{\tau_I}\int Edt + \tau_D\frac{dE}{dt}\right) \tag{18}$$

The controller parameters, K_c,$\tau_{I,\ and}$ τ_D, affect the response of the controller. These parameters can be determined using various techniques. In this study, Relay–Feedback Testing and Ziegler–Nichols method [18] are used.

With a thermal storage design, the SMDDS can be divided into two subsystems, the solar thermal subsystem and the membrane distillation subsystem, and interconnected via the heat exchanger. The control structure is developed for each subsystem with the aim of meeting the target temperatures of inlet streams to the heat exchanger. For the solar thermal subsystem, with fixed circulation flow rate of solar thermal loop ($m_{f,STL}$), the flow rate entering the thermal storage tank is chosen as the manipulated variable. For the membrane distillation, the manipulated variable is the feed water flow rate. The fluid circulation routes in the solar thermal subsystem under daytime and nighttime are different, because the fluid will not flow through the solar absorber when no solar irradiation. The dynamic characteristics during daytime and nighttime operations will then be different. Therefore, one temperature controller is allocated for

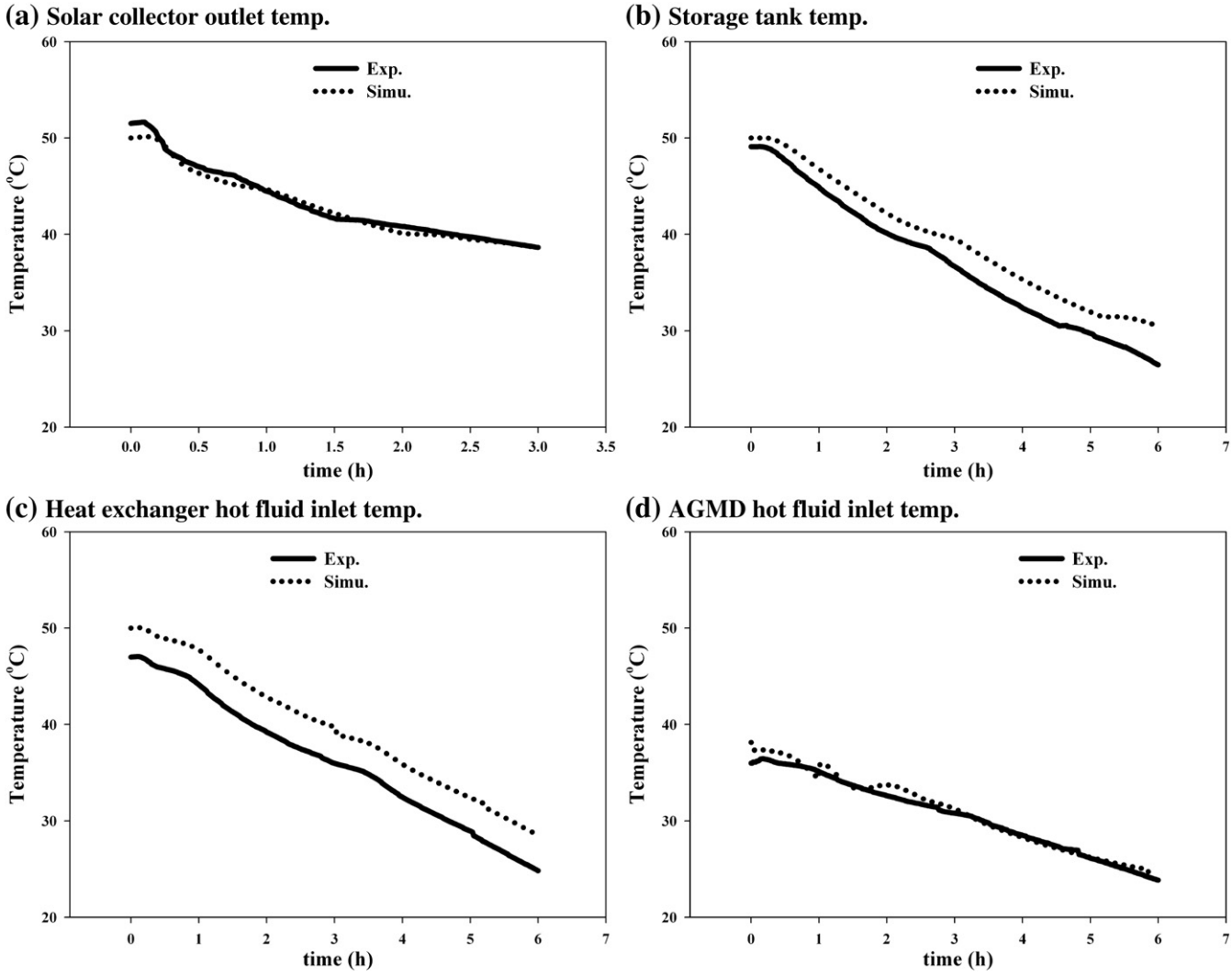

Fig. 6. Base case temperature profiles for cloudy day.

each type of operation. The controller loops are shown in Fig. 1(a). PI controllers, instead of PID controllers, are employed because the use of derivative control generally will cause greater fluctuation in response.

In the experimental setup, which uses a thermostat to simulate the solar absorber, the control system design for fully automatic operation is simpler. For a system which uses solar absorber, a complete control system design for a fully automatic SMDDS is proposed and illustrated

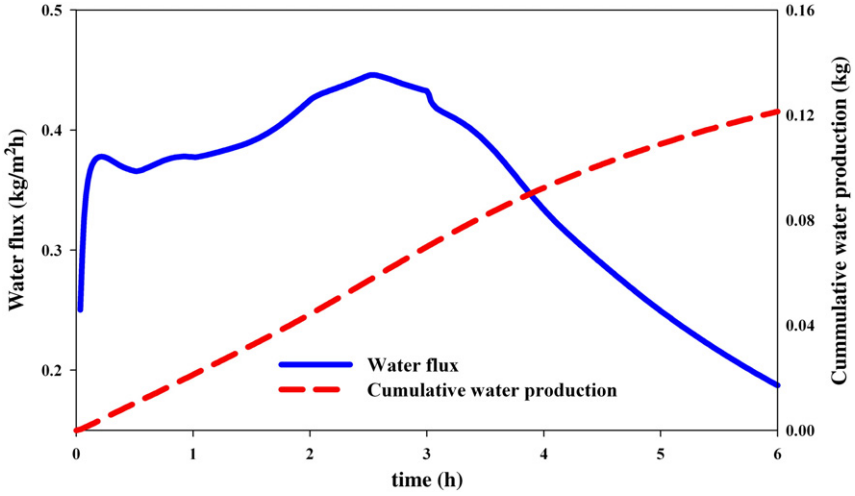

Fig. 7. Base case water flux and production rate for sunny day.

in Fig. 4 and Table 2. In addition to the abovementioned three PI temperature controllers, ON-OFF controllers are allocated to turn on or off the pumps as well as the fluid circulations to the solar absorber and to the thermal storage tank for daytime and nighttime. These ON–OFF controllers are operated based on the temperature difference between the solar absorber and its circulation fluid or on the temperature in the thermal storage tank. Based on the comparison of the temperatures of solar absorber and its circulation fluid, the ON–OFF controllers will switch the operation mode between daytime and nighttime. The system can be shut down based on the temperature of the thermal storage tank, when it is lower than a set value. The control devices and settings are summarized in Table 2.

5. Model verification

The simulation and experimental results are compared for a base case under manual operation and automatic control. For manual operation, the operating conditions of $m_{f,STL}$, $r_{f,ST}$ and $m_{f,MD}$ are fixed at 4.8 kg/h, 0.7 and 2.4 kg/h. The initial temperatures of thermal storage tank and inlet water to the membrane distillation module are 50 °C and 20 °C. For automatic operation, $r_{f,ST}$ and $m_{f,MD}$ are adjusted by the PI controllers.

For manual operation under sunny day and cloudy day, the temperature profiles of four major points are obtained from experiment and simulation and are compared in Figs. 5 and 6, respectively. For all four measuring points, the trends of temperature variation with time from experiment and simulation are fairly close. However, for the storage tank and heat exchanger hot fluid inlet stream, as shown in Figs. 5(b), (c), (b) and 6(c), the temperatures from experiment are constantly lower by several degrees than the simulation ones. The reason is probably due to the heat loss from these equipments to the ambient. For sunny day, all temperature profiles show peaks at about 0.5–1 h later than the irradiation profile. The highest temperature of the system occurs at the outlet from the solar absorber (hot thermostat) and reaches only 55 °C. The highest inlet temperature of hot fluid to the membrane distillation module is 40.6 °C. The large the temperature difference between these two points results from two factors. One is the fluid circulation pattern between the solar absorber, storage tank and the heat exchanger. Only part of the fluid leaving the solar absorber enters the heat exchanger, rest of the fluid is sent to the storage tank. The other one is the temperature difference between the hot and cold fluids in the heat exchanger. The final temperatures of the storage tank are about 30 °C. These low temperature levels indicate that the circulation flow rate of the solar thermal loop ($m_{f,STL}$) is too high. Reducing the flow rate could raise the peak temperatures as well as the peak water

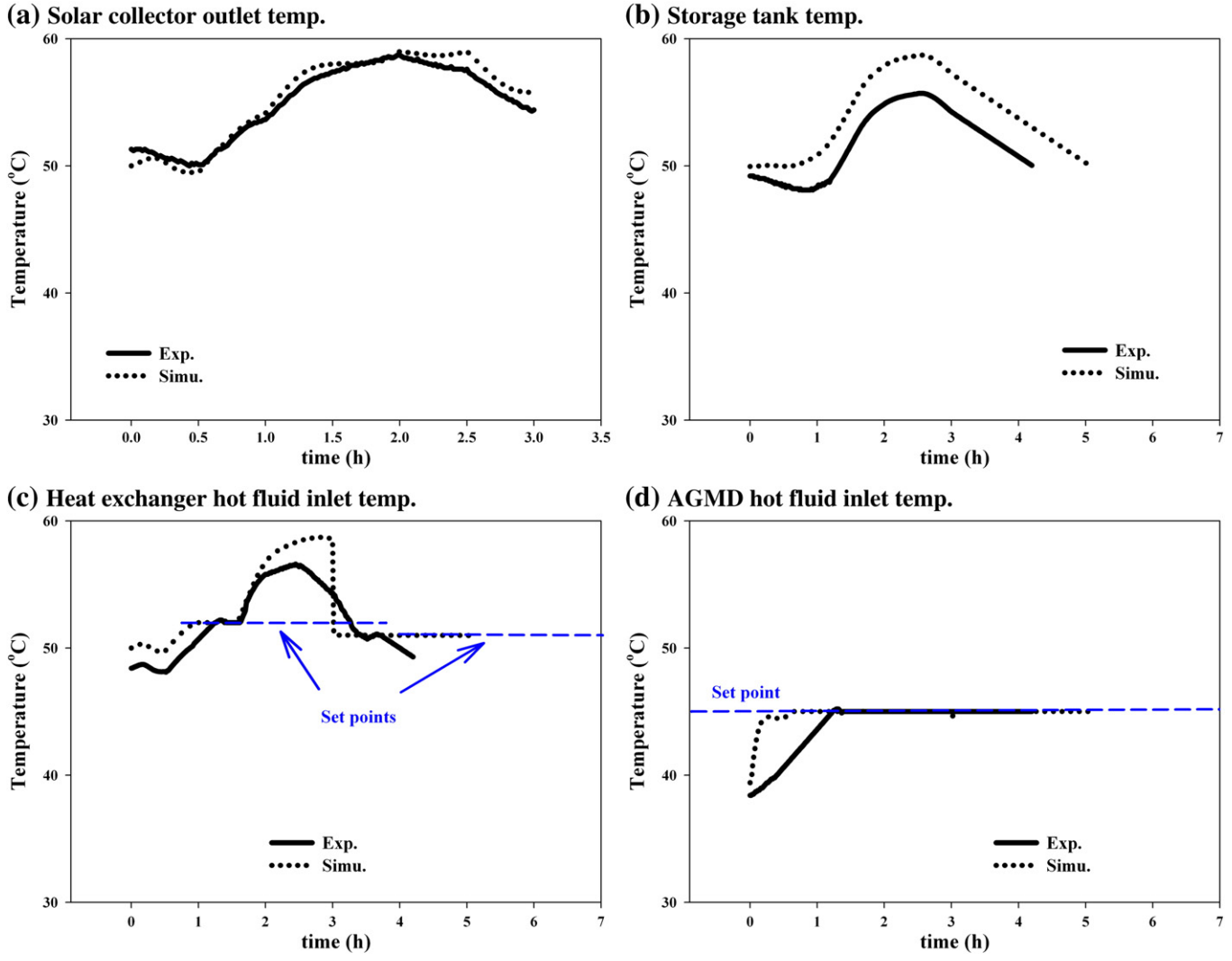

Fig. 8. Temperature profiles with controller set point 1 for sunny day.

production rate. For cloudy day, due to the low solar irradiation energy, the temperature decreases with time for all the streams, as shown in Fig. 6. The water flux and cumulative water production for sunny day operation are shown in Fig. 7, the water flux keeps at a relatively constant level for the 3-hour daytime period.

For automatic operation study, two sets of set points for the controllers are analyzed. The set point 1 sets 52 °C/51 °C and 45 °C for TC1(daytime)/TC2(nighttime) and TC3, respectively. The set point 2 sets 52 °C/51 °C and 40 °C for TC1(daytime)/TC2(nighttime) and TC3, respectively. TC1 and TC2 can adjust the flow entering the thermal storage tank to meet their set point temperatures. TC3 can manipulate the operation flow rate of membrane distillation module. The control system will shut down the operation when the temperature of the storage tank is dropped to 50 °C. The comparisons of temperature profiles for sunny day operation are given in Figs. 8 and 9. The simulation results, as shown in Figs. 8(c) and 9(c), indicate that the temperature of the inlet hot fluid of heat exchanger can be maintained at set point for a short time period only during daytime but for the entire operating period during nighttime. For a period of about 1 h which corresponds to the highest irradiation period, the temperature is much higher than the set point. This reveals the improper setting of the set point temperature, specifically the set point for daytime (52 °C) is too low. Even when the exit fluid from solar absorber is totally sent to the tank, the temperature of the fluid entering the heat exchanger cannot be reduced to the set point. The experimental results show similar profiles with the simulation, however, the time periods of meeting the set point are much shorter. These outcomes should be resulted from the heat losses of the equipments, as can be seen from Figs. 8(b) and 9(b). For the membrane distillation subsystem, the control results are much better as seen from Figs. 8(d) and 9(d). Both experimental and simulation results show controlled temperature on the set point.

6. Optimal operation

With the mathematical model developed in this study, the optimal operation for obtaining the maximum daily water production can be analyzed. The definition of the optimization problem is to maximize the cumulative daily water production under given solar irradiation condition and solar thermal loop circulation rate ($m_{f,STL}$). The decision variables are the feeding rate to the thermal storage tank and the flow rate of membrane distillation operation. The optimization solver FEASOPT (feasible path successive quadratic programming optimization) in Aspen Custom Modeler® [12] is used for the analysis. The optimization results for the solar thermal loop circulation rate of 2.4 kg/h are

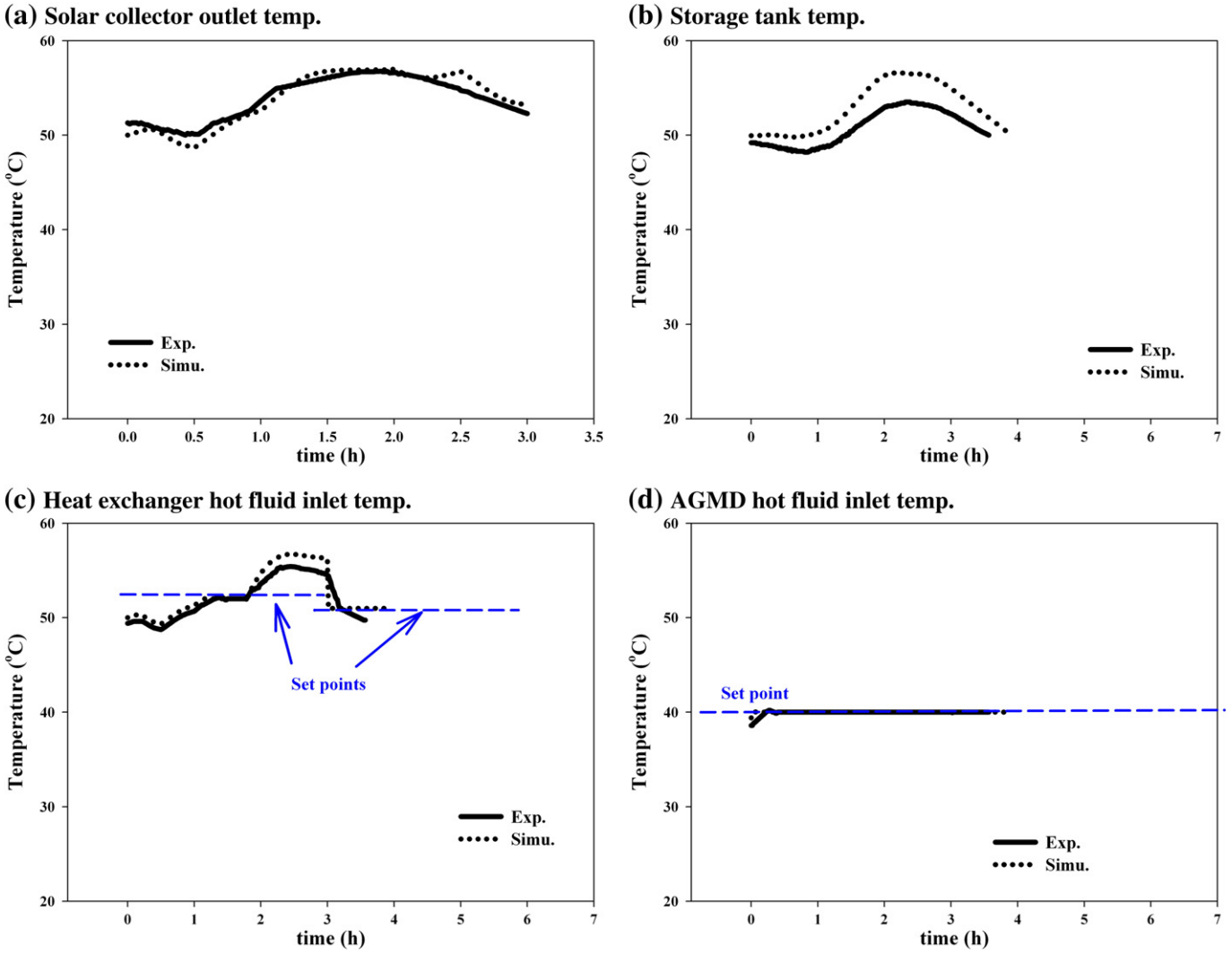

Fig. 9. Temperature profiles with controller set point 2 for sunny day.

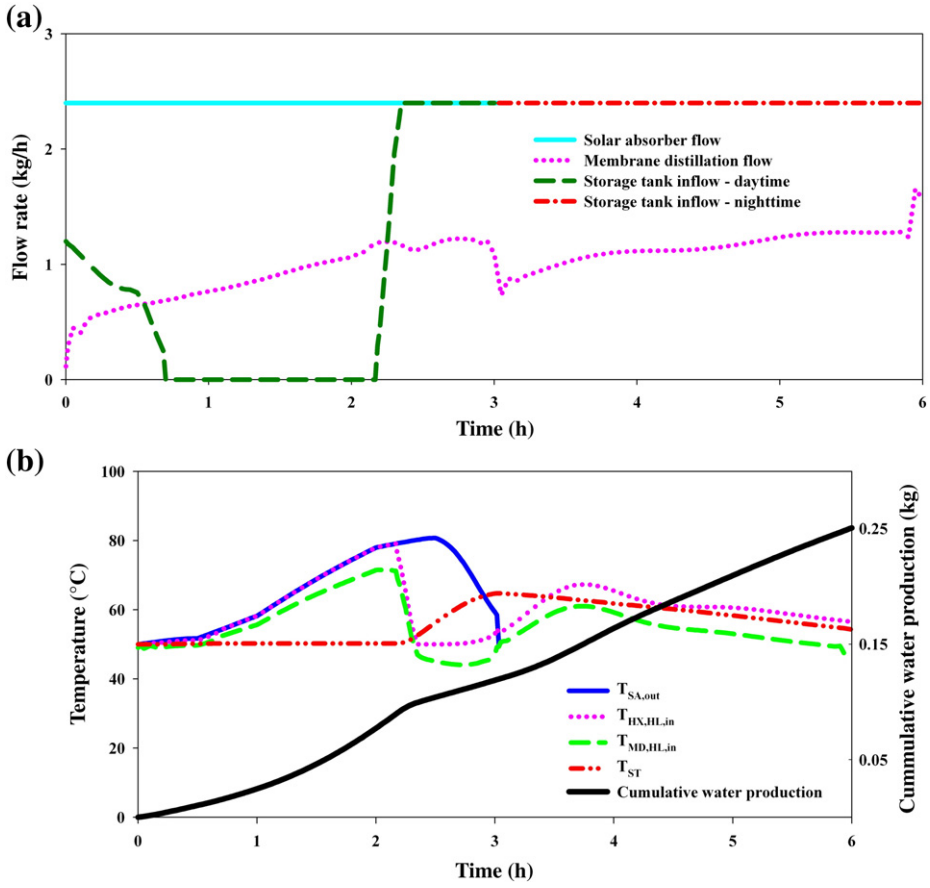

Fig. 10. Temperature and flow profiles of optimal operation for sunny day.

presented in Figs. 10 and 11. For sunny day, as shown in Fig. 10(a), the optimal operation should adopt the following strategy:

- For the entire daytime period, the circulation fluid should be sent to the solar absorber.
- For the early morning (first hour) period, operates with a small part of thermal circulation fluid entering the thermal storage tank.
- For the mid-day (second hour) period, which has the highest irradiation strength, operates with no thermal storage to the tank. That is to send all the thermal circulation fluid directly to the heat exchanger.
- For the rest of daytime hours, which have low solar irradiation, operates with the entire circulation fluid entering the storage tank.
- For the entire period, the flow of membrane distillation subsystem should be maintained at an approximately constant level, about 1 kg/h.

The temperature profiles, Fig. 10(b), show peaks both during daytime and nighttime with the second peak resulted from starting of utilizing the stored thermal energy in the tank. The cumulative water product curve is close to linear, indicating a constant water production rate.

For cloudy day, as shown in Fig. 11(a), the optimal operation should employ the following strategy:

- The fluid should be sent to the solar absorber only when the irradiation is high enough.
- Even during the period when the solar absorber is operating, part of the thermal energy must be supplied by the storage tank.
- For the entire period, the flow of membrane distillation subsystem should be maintained at an approximately constant level, about 1 kg/h.

The temperature profiles, Fig. 11(b), all show a similar trend of descending with time. The peaks at the end of daytime are the outcome of reusing the fluid in the storage tank. The cumulative water product curve is linear, indicating a constant water production rate.

For comparison purpose, the system under automatic control is simulated with the set point temperatures for the controllers determined based on the optimization analysis. Using the average temperatures during daytime and nighttime, the set points are set to be 63 °C/61 °C and 55 °C for TC1(daytime)/TC2(nighttime) and TC3, respectively. The results from automatic control operation and optimal operation are compared in Table 3. Using automatic operation, the water production is about 80% of the optimal operation under sunny day and the final temperature in the storage tank and total operating hours from both types of operation are close. But for cloudy day, the automatic operation gives very low water production and total operating hours due to the system shut down after the temperature of storage tank is lower than the preset 50 °C.

7. Conclusions

The performance of a SMDDS has been analyzed by both experimental and simulation approaches. The mathematical model, which is verified by dynamic experimental data, provides a convenient and powerful tool for the analysis and design of the system. The control scheme developed allows fully automatic operation of the system under variable solar irradiation conditions. The optimization analysis using the model provides information for operation strategies for sunny day and cloudy day. For sunny day, the performance of the control system is closed to 80% of the maximum obtainable water production from optimizaton study.

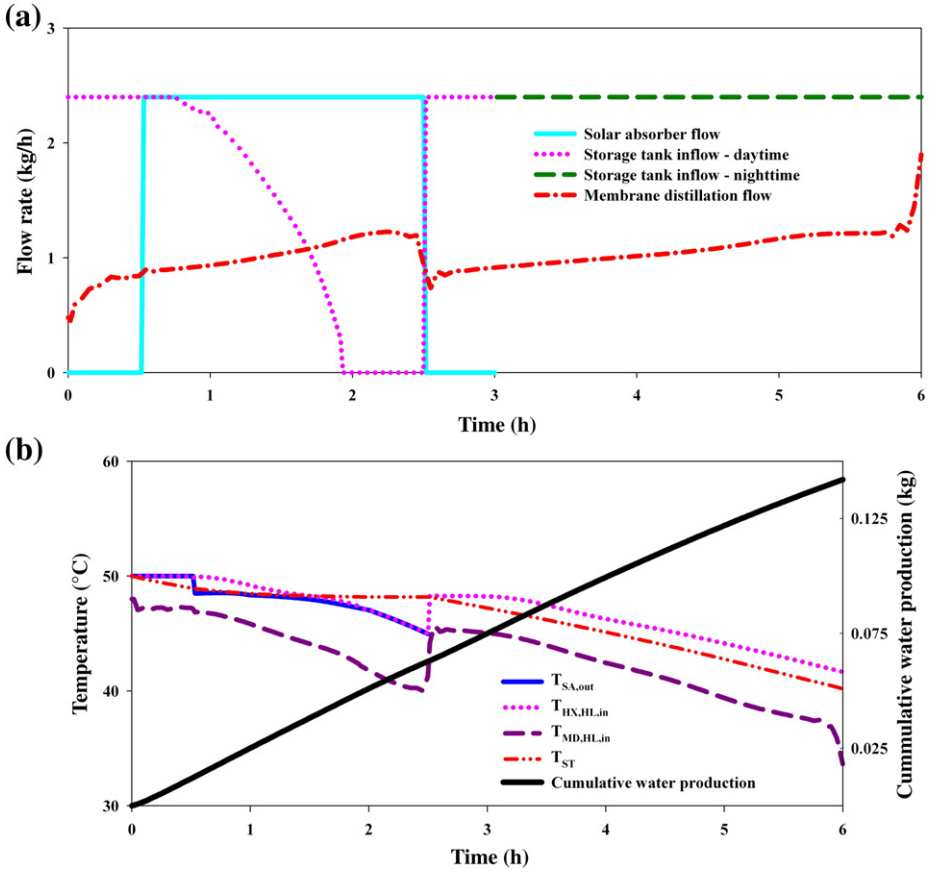

Fig. 11. Temperature and flow profiles of optimal operation for cloudy day.

Table 3
Comparison of performances from automatic and optimal operations.

Solar irradiation/operation mode	Water production rate (kg/day)	Temperature of thermal storage tank at the end of daily operation (°C)	Total daily operation hours (h)
Sunny/control	0.2	55.4	6
Sunny/optimal	0.248–0.258	53.9–54.3	6
Cloudy/control	0.03	50	2.5
Cloudy/optimal	0.142	40.2	6

Note: Solar thermal loop circulation rate is 2.2–3.0 kg/h.

Symbol

A	Area (m^2)
Cp	Heat capacity (J/kg K)
D_m	Molecular diffusivity (m^2/s)
D_K	Kundsen diffusivity (m^2/s)
d_p	Membrane pore diameter (μm)
E	Error in PID controller
H	Height (m)
h	Heat transfer coefficient (W/m^2 K)
I	Intensity of solar irradiation (W/m^2)
K_c	Proportional gain for PID controller
k	Mass transfer coefficient (m/s)
L	Length of the equipment (m)
M	Mass of the fluid in the module (kg)
M_w	Molecular weight of water (kg/kmol)
m	Mass flow rate (kg/s)
N	Mole flux of water (kmol/m^2 s)
OP	Output of PID controller
P	Pressure (Pa)
Q_h	Heat transfer rate by convection or conduction (J/s)
Q_N	Heat transfer rate by the temperature change of the water flux (J/s)
R	Gas constant (Pa m^3/kmol K)
Re	Reynolds number
r	Ratio (−)
T	Temperature (K)
$\bar{T}$	Average Temperature (K)
t	time
U	Overall heat transfer coefficient (W/m^2 K)
W	Width of the equipment (m)

Greek letters

ΔH_{VL}	Enthalpy for vapor–liquid phase change (J/m^2 s)
ΔH_{vap}	Heat of vaporization (J/kmol)
ΔT	Temperature difference (K)
δ	Thickness (m)
ε	Porosity of the membrane

τ	Tortuosity of the membrane
τ_D	Derivative gain for PID controller
τ_I	Integral gain for PID controller

Superscripts

L	Liquid
sat	Saturation
T	Total
V	Vapor

Subscripts

ag	Air gap
CL	Cold liquid
cp	Cooling plate
CONL	Condensing liquid
f	Fluid
HL	Hot liquid
HX	Heat exchanger
in	Inlet
j	Heat or mass transfer layer
lf	Liquid film
lm	Logarithmic mean
MD	Membrane distillation module
m1	Hot fluid-membrane interface
m2	Membrane-air gap interface
mem	Membrane
out	Outlet
SA	Solar absorber
ST	Thermal storage tank
STL	Solar thermal loop
w	Water

Acknowledgment

The authors gratefully acknowledge the sponsorship from the National Science Council of Taiwan (NSC-99-2621-M-032-002).

References

[1] F. Banat, N. Jwaied, M. Rommel, J. Koschikowski, M. Wieghaus, Performance evaluation of the "large SMADES" autonomous desalination solar-driven membrane distillation plant in Aqaba, Jordan, Desalination 217 (2007) 17–28.
[2] F. Banat, N. Jwaied, M. Rommel, J. Koschikowski, M. Wieghaus, Desalination by a "compact SMADES" autonomous solar-powered membrane distillation unit, Desalination 217 (2007) 29–37.
[3] F. Banat, N. Jwaied, Economic evaluation of desalination by small-scale autonomous solar-powered membrane distillation units, Desalination 220 (2008) 566–573.
[4] G.W. Meindersma, C.M. Guijt, A.B. de Haan, Desalination and water recycling by air gap membrane distillation, Desalination 187 (2006) 291–301.
[5] E. Guillén-Burrieza, J. Blanco, G. Zaragoza, D.C. Alarcón, P. Palenzuela, M. Ibarra, W. Gernjak, Experimental analysis of an air gap membrane distillation solar desalination pilot system, J. Membr. Sci. 379 (2011) 386–396.
[6] J.B. Gálvez, L. García-Rodríguez, I. Martín-Mateos, Seawater desalination by an innovative solar-powered membrane distillation system: the MEDESOL project, Desalination 246 (2009) 567–576.
[7] H. Ben Bacha, M. Bouzguenda, T. Damak, M.S. Abid, A.Y. Maalej, A study of a water desalination station using the SMCEC technique: production optimization, Renew. Energy 21 (2000) 523–536.
[8] L. Roca, M. Berenguel, L. Yebra, D.C. Alarcón, Preliminary modeling and control studies in AQUASOL project, Desalination 222 (2008) 466–473.
[9] H. Chang, J.-S. Liau, C.-D. Ho, W.-H. Wang, Simulation of membrane distillation modules for desalination by developing user's model on Aspen Plus platform, Desalination 249 (2009) 380–387.
[10] H. Chang, G.-B. Wang, Y.-H. Chen, C.-C. Li, C.-L. Chang, Modeling and optimization of a solar driven membrane distillation desalination system, Renew. Energy 35 (2010) 2714–2722.
[11] H. Chang, C.-L. Chang, C.-D. Ho, C.-C. Li, P.-H. Wang, Experimental an.lkd simulation study of an air gap membrane distillation module with solar absorption function for desalination, Desalin. Water Treat. 25 (2011) 251–258.
[12] Aspen Technology, Inc. Massachusetts, USA.
[13] E.L. Cussler, Diffusion: Mass Transfer in Fluid Systems, 2nd Ed. Cambridge University Press, 1997.
[14] S. Bouguecha, R. Chouikh, M. Dhahbi, Numerical study of the coupled heat and mass transfer in membrane distillation, Desalination 152 (2002) 245–252.
[15] J. Holman, Heat Transfer, McGraw-Hill, 1989.
[16] D. Al-Gobaisi, A. Barakzai, A. El-Nashar, An overview of modern control strategies for optimizing thermal desalination plants, Desalination 84 (1991) 3–43.
[17] I. Alatiqi, H. Ettouney, H. El-Dessouky, Process control in water desalination industry: an overview, Desalination 126 (1999) 15–32.
[18] W. Luyben, M. Luyben, Essentials of Process Control, McGraw-Hill, 1997.